IEEE Access
Multidisciplinary | Rapid Review | Open Access Journal

Received January 30, 2021, accepted February 12, 2021, date of publication February 22, 2021, date of current version March 5, 2021.

Digital Object Identifier 10.1109/ACCESS.2021.3061117

Parameters Selection Method of Circuit Breaker and Fault Current Limiter in Mesh-Type DC Microgrid

LIANG KONG AND HENG NIAN, (Senior Member, IEEE)
College of Electrical Engineering, Zhejiang University, Hangzhou 310027, China
Corresponding author: Heng Nian (nianheng@zju.edu.cn)

This work was supported by the National Key Research and Development Program of China under Grant 2017YFB0903300.

ABSTRACT Circuit breaker (CB) and fault current limiter (FCL) are two major fault protection devices used in mesh-type DC microgrids. This paper proposes the parameters selection method to obtain a reliable and economic configuration scheme of CBs and FCLs applied in mesh-type DC microgrid. The breaking time of CB, the nominal breaking current of CB and the inductance of FCL are selected as three optimization parameters in an evaluation model. Since the reliability of fault protection scheme depends on whether the nominal breaking current of the CB is greater than the line current at the breaking moment of CB, it is necessary to accurately calculate the post-fault line current. Based on this, an accurate transient DC microgrid model is presented in this paper. And then, an improved non-dominated sorting genetic algorithm II (NSGA-II) is used to configure the parameters of CBs and FCLs quickly. Besides, a case study on six-terminal DC microgrid test system shows that the proposed method can obtain accurate post-fault line current and can achieve the parameters selection of CBs and FCLs.

INDEX TERMS Mesh-type DC microgrid, DC fault, circuit breaker, fault current limiter, parameters selection.

I. INTRODUCTION

The DC microgrid is a promising application in the electric power system. Firstly, there are no concepts of phase and reactive power in DC microgrids, so that renewable power generation system can be connected to AC/DC hybrid distribution system through DC microgrid without considering phase synchronization [1]. Secondly, some devices (such as photovoltaics, energy storage) are more suitable to connect to the AC/DC hybrid distribution system through DC microgrid [2], [3]. Moreover, the application of DC microgrids enables transmission power can be flexibly controlled in AC/DC hybrid distribution system. It can ensure efficient access of devices during normal operation and can achieve fast cross-region power support in emergency situations [4]–[6]. Therefore, compared with the traditional AC grid, the DC microgrid has many advantages and grows rapidly.

Since the impedance of lines in DC microgrid is less than that in AC grid, the influence caused by short circuit fault in DC microgrid is more serious than that in AC grid [7], [8]. Since the faulty current in DC microgrid has no zero crossing, it is more difficult to cut off the faulty line than that in AC grid [1]. Thus, fault protection of DC microgrid has become a significant challenge for the development of AC/DC hybrid distribution system. There have been preliminary studies on fault protection of DC microgrid which generally use circuit breakers (CBs) to isolate the fault in DC microgrid [9]–[12]. The post-fault lines current in DC microgrid may increase rapidly and even exceed the nominal breaking current of CB before the breaking time [13]. To isolate faulty segment by CB successfully, the fault current limiter (FCL) has been used to limit the rise rate of faulty current after fault occurs in DC microgrid referring to the method of HVDC grid in [14].

The technology of CB and FCL was comprehensively reviewed [15]. CB is used to break faulty lines, and there are three types of CB, i.e., Mechanical CB (MCCB) [16], Solid-state CB (SSCB) [17] and Hybrid mechanical-solid CB (HMSCB) [18]. Since the MCCB uses the traditional AC mechanical breaking unit to break the faulty line, their fault interruption time is as slow as 30-100 milliseconds. This breaking speed cannot meet the requirements of DC

The associate editor coordinating the review of this manuscript and approving it for publication was Hazlie Mokhlis.

microgrid. The SSCB uses the controllable breaking characteristics of solid-state switch to break the faulty line, which makes the SSCB can break the faulty line quickly. However, the SSCB has considerable conduction losses in steady state. The HMSCB combines the advantages of the previous two CBs. Current flows through the branch with mechanical switch in steady state and the branch with solid-state switch in faulty condition. This decrease the losses of HMSCB and breaks the faulty line rapidly. Due to the excellent performance of HMSCB, it is suitable for HVDC and DC microgrid. Thus, HMSCB was selected as the analysis object.

FCL is used to limit the faulty current and can be divided into three types, i.e., Resistive-superconducting FCL (SFCL) [19], Solid-state FCL (SSFCL) [20] and Inductor-type FCL (IFCL) [7]. The current-limiting device in SFCL usually employs a superconducting resistor, which has a low resistance in steady state, and can be transformed into a high resistance when a fault occurs. Although SFCL has superior performance, special low-temperature device is required in SFCL. Thus, it is only suitable for HVDC, and still considered as immature and costly for DC microgrid. The current limiting principle of SSFCL is the same as the breaking principle of SSCB, so SSFCL can be regarded as an additional function of SSCB. Since the solid-state switch in SSFCL needs to be adjusted by the control system, there is a time delay in the current limiting, which cannot suppress the instantaneous rising of faulty current. In addition, since SSFCL is an additional function of SSCB, it is not suitable as a main current limiting device. IFCL can be regarded as a reactor connected in series in the line. Although the installation of IFCL will increase the electrical distance of DC system, IFCL has low cost and high reliability, and is very suitable for DC microgrids. On this basis, IFCL was selected as the analysis object.

With the development of DC microgrid, the topology of DC microgrid changes from radial-type [9] or ring-type [10]–[12] to mesh-type. The radial-type DC microgrid is the simplest DC microgrid, and there are no loops in the structure. Thus, there is no coupling relationship between the lines. The ring-type DC microgrid has a loop in the structure. This means that there are two paths for power transmission between any terminal and the fault position. The coupling of mesh-type DC microgrid is more significant than that in radial-type and ring-type DC microgrid, so that the mesh-type DC microgrid has a better redundancy, flexibility and reliability, and provides the possibility for the expansion of DC microgrid capacity. A comparison of those three types for post fault transient behavior is shown in Table 1. However, compared with radial-type and ring-type topologies, more CBs and FCLs need to be installed in mesh-type DC microgrid. Therefore, it is significant to develop parameters selection method of CBs and FCLs in mesh-type DC microgrid to protect DC microgrid accurately and quickly.

Different from DC microgrid, the selection of CBs and FCLs parameters in mesh-type AC grid has been widely studied. In order to implement the selection of CBs and FCLs in AC grids, the post-fault transient model is established firstly and the model of faulty current under the consideration of FCLs is developed. And then, the parameters of CBs and FCLs can be optimized by heuristic algorithms, i.e., genetic algorithm (GA) [21], [22], Particle Swarm Optimization (PSO) [23], [24], harmony search algorithm [25].

TABLE 1. Comparison of different types DC microgrid for transient behavior.

Structure	Transient Behavior
Radial-type	No coupling relationship between the lines, easy to analyze.
Ring-type	Having a loop in the structure, existing two paths between any terminal and the fault position.
Mesh-type	The lines are coupled to each other, the most difficult to analysis.

Based on the design method of CBs and FCLs parameters in AC grids, a parameters selection method of CBs and FCLs in DC microgrid is proposed in [13], in which an evaluation model of CBs and FCLs is established and solved by GA algorithm. Furthermore, analytical expressions of faulty current are deduced. However, not all parameters related to short circuit fault in CBs and FCLs are considered in the evaluation model in [13] (such as the breaking time of CBs). Besides, the transient model of DC microgrid in [13] lacks the consideration of the intermediate nodes.

Under this situation, a parameters selection method of CBs and FCLs in mesh-type DC microgrid is proposed in this paper. The main contributions of the proposed parameters selection method can be described as following: 1) An evaluation method considering all parameters of CBs and FCLs is developed, and the parameters in hybrid mechanical-solid CB and inductor-type FCL were optimized as an example; 2) An accurate transient DC microgrid model considering the intermediate nodes in mesh-type topology is established in difference equation form; 3) An improved NSGA-II algorithm considering the calculation of non-dominated sorting and crowding distance is proposed to accelerate convergence of iteration in the parameter selection.

The rest of this paper is organized as follows. Section II presents the parameters selection problem of CBs and FCLs in mesh-type DC microgrid. And the evaluation model of CBs and FCLs is introduced in Section III. Next, Section IV gives the process of parameters selection method, establishes the transient DC microgrid model, and improves the NSGA-II algorithm. And then, the proposed parameters selection method of CBs and FCLs is validated in Section V. Finally, Section VI draws the conclusion.

II. PROBLEM STATEMENT

In order to describe the mesh-type DC microgrid clearly, a six-terminal mesh-type DC microgrid test system is established in this section. And the operation principles of CB and FCL are shown in this test system.

A. SIX-TERMINAL DC MICROGRID TEST SYSTEM

Referring to the large onshore renewable power generation grid (DCS-A) in DCS-M [26], the schematic diagram of the

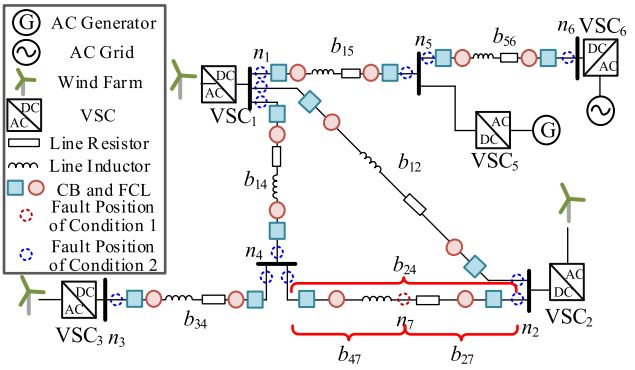

FIGURE 1. The schematic diagram of mesh-type DC microgrid test system.

TABLE 2. Parameters of DC Lines.

Line	Length(km)	Resistance(Ω)	Inductance(mH)
1-2	2	0.12	1.92
1-4	3	0.18	2.88
1-5	3	0.18	2.88
2-4	4	0.24	3.84
3-4	1	0.06	0.96
5-6	3	0.18	2.88

test system is shown in Fig. 1. There are six nodes in the mesh-type DC microgrid test system. The nodes n_1, n_2, n_3, n_5 and n_6, which connect to voltage source converter (VSC) directly, are defined as ''real nodes''. The node n_4, which connects to VSC indirectly, is defined as ''intermediate node''.

The parameters of DC lines include DC-links capacitance, lines resistance and lines inductance. Referring to [27], the parameters are set as follows. The DC-links capacitances of all nodes are 9000μF. The resistance and inductance of DC lines are proportional to their lengths and shown in Table 2.

The master-slave control is taken as the example control strategies to verify the parameters selection method proposed by this paper. A detailed description of the master-slave control can be found in [28]. DC-link voltage control is used in VSC connected to AC generator, while active power control is used in VSC connected to AC grid or wind farm. Based on that, the DC voltage reference of VSC_5 is set as 1000V. The input power references of VSC_1, VSC_2, VSC_3 are set as 100kW respectively. The output power reference of VSC_6 is set as 400kW. By calculating the steady-state power flow of the six-terminal mesh-type DC microgrid, the steady-state nodes voltage and lines current can be obtained, as shown in Table 3.

B. OPERATION PRINCIPLES OF CB AND FCL IN DC MICROGRID

Since the pole-to-pole fault is more serious than the pole-to-ground fault, the pole-to-pole fault is chosen as the analyzed fault in this paper. As shown in Fig. 1, CBs and FCLs are used as protection devices and installed at both ends of each DC line. Assuming that a short circuit fault occurs at the midpoint of b_{24} (fault condition 1), and the faulty position is defined

TABLE 3. Steady-state nodes voltage and lines current.

Node	1	2	3	4	5	6
Value(V)	1052	1064	1072	1066	1000	923
Line	1-2	1-4	1-5	2-4	3-4	5-6
Value(A)	-104	-83	280	-10	93	435

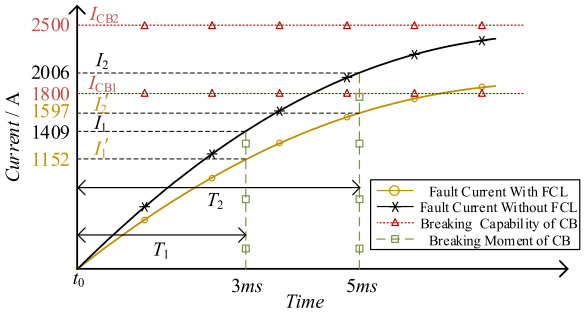

FIGURE 2. Line current after a short circuit fault occurs on a DC line.

TABLE 4. Lines breaking situations under different parameters of CBs and FCLs.

CB / FCL	5ms 1800A	5ms 2500A	3ms 1800A	3ms 2500A
Without FCL	×	√	√	√
2mH FCL	√	√	√	√

as node 7. Moreover, the fault resistance is zero. The faulty current of line 2-7 without and with 2mH FCLs are shown in Fig. 2. Meanwhile, two kinds of breaking time of CBs (3ms and 5ms) and two kinds of nominal breaking current of CBs (1800A and 2500A) are also marked in Fig. 2.

As shown in Table 4, if the FCL is not equipped, the faulty segment cannot be broken by a CB with the breaking time T_2 (5ms) and the breaking capacity I_{CB1} (1800A). However, the faulty segment can be broken by reducing T_2 (5ms) to T_1 (3ms), increasing I_{CB1} (1800A) to I_{CB2} (2500A), or equipping 2mH FCL on the faulty line. This indicates that the breaking of fault segment is realized through the cooperation of CB and FCL.

The cost of each CB is related to the breaking time and the nominal breaking current. It should be noted that, the shorter the breaking time and the higher the nominal breaking current, the higher the cost of CB. And the cost of FCL is directly proportional to inductance of FCL. Though the faulty segment can also be broken by CB (3ms, 2500A) and FCL (2mH), this cooperation has the highest cost and the worst economy. Thus, it is significant to select suitable CBs and FCLs which take both reliability and economy into consideration.

III. EVALUATION MODEL OF CBS AND FCLS

The short circuit parameters of CBs and FCLs are analyzed in this section. Furthermore, referring to parameter selection principles of CBs and FCLs in AC grids [21]–[25], the

objective functions and status conditions of that in mesh-type DC microgrid are established.

A. SHORT CIRCUIT PARAMETERS OF CB AND FCL

Various electrical devices have different functions and different working conditions, so the selection of parameters is also different.

CBs in DC microgrid need to select 8 parameters: nominal voltage, nominal current, thermal current, dynamic current, nominal breaking current, nominal closing current, breaking time, and close time. Among these 8 parameters, the parameters related to short circuit fault are nominal breaking current and breaking time. And these two parameters can be selected as the optimization object.

FCLs in DC microgrid need to select 7 parameters: nominal voltage, nominal current, thermal current, dynamic current, inductance, voltage drop during normal operation, and residual voltage after short circuit. Among these 7 parameters, the parameters related to short circuit fault are inductance, voltage drop during normal operation, and residual voltage after short circuit. And the inductance can be selected as the optimization object. The voltage drop during normal operation and residual voltage after short circuit are parameters that are used as constraints.

B. OBJECTIVE FUNCTION

The objective functions are divided into economy objective function and reliability objective function. The economy objective function includes the cost of CBs and FCLs. As the analysis in Section II.B, the cost of each CB is related to the breaking time and the nominal breaking current. The objective functions of CBs can be expressed as:

$$\begin{cases} \text{Max}\, f_1 = \sum_{i=1}^{N_{CB}} F_i \\ \text{Min}\, f_2 = \sum_{i=1}^{N_{CB}} I_i \end{cases} \tag{1}$$

where F_i is the length of breaking time of CB_i, I_i is the nominal breaking current of CB_i, N_{CB} is the number of CBs.

As the analysis in Section II.B, the objective function of FCLs can be expressed as:

$$\text{Min}\, f_3 = \sum_{j=1}^{N_{FCL}} X_j \tag{2}$$

where X_j is the inductance of FCL_j, N_{FCL} is the number of FCLs.

In order to sort schemes that cannot break the fault line reliably. The constraints of whether the current of line exceeds the breaking current are converting into a total objective function. Furthermore, this process is beneficial to find schemes that satisfy all constraints in iteration. The reliability objective function can be expressed as:

$$\text{Min}\, f_4 = \sum_{i=1}^{N_{CB}} E_i \tag{3}$$

where E_i is the judgement of whether the current $I_{i,line}$ of line i exceeds the nominal breaking current $I_{i,CB}$ of CB_i.

$$E_i = \begin{cases} 0 & \text{if } I_{i,line} < I_{i,CB} \\ 1 & \text{otherwise} \end{cases} \tag{4}$$

C. STATUS CONSTRAINTS

1) EQUALITY CONSTRAINT

The status constraints are divided into power constraint, capacity constraints and voltage drop constraints. The power constraint means that the active power balance of each node. And power constraint can be expressed as:

$$P_i = U_i \sum_{j=1}^{N_b} \left(U_i - U_j\right) / R_{ij} \tag{5}$$

where U_i is the voltage of node i, R_{ij} is the resistance between node i and node j, N_b is the number of lines connected to node i, P_i is the power of node i injected from VSC.

2) INEQUALITY CONSTRAINTS

The capacity constraints refer to the selection range of CBs and FCLs parameters, which can be expressed as:

$$T_{i,CB}^{\min} \le T_{i,CB} \le T_{i,CB}^{\max} \tag{6}$$

$$I_{i,CB}^{\min} \le I_{i,CB} \le I_{i,CB}^{\max} \tag{7}$$

$$X_{j,FCL}^{\min} \le X_{j,FCL} \le X_{j,FCL}^{\max} \tag{8}$$

where $T_{i,CB}$ is the breaking time of CB_i. $I_{i,CB}$ is the nominal breaking current of CB_i. $X_{j,FCL}$ is the inductance of FCL_j. Symbols with superscripts of ''max'' or ''min'' represent the maximum limit or minimum limit of corresponding parameters.

The voltage drop constraints refer to the voltage drop during normal operation and residual voltage after short circuit. There is an upper limit of the voltage drop during normal operation, which can be expressed as (9). Meanwhile, there is a lower limit of the residual voltage after short circuit, which can be expressed as (10).

$$\Delta U_i\% = \frac{\Delta U_i}{U_{iN}} \times 100 \le A_i \tag{9}$$

$$\Delta U_{i\_re}\% = \frac{\Delta U_{i\_re}}{U_{i\_N}} \times 100 \ge B_i \tag{10}$$

where ΔU_i is the voltage drop of node i, ΔU_{i_re} is the residual voltage of node i, U_{i_N} is the nominal voltage of node i, A_i is the upper limit of the voltage drop of node i, B_i is the lower limit of the residual voltage of node i.

IV. PARAMETERS SELECTION METHOD

The parameters selection method of CBs and FCLs is described in detail in this section. Firstly, an accurate fault transient model of mesh-type DC microgrids is developed in this section. And it is the key to obtain the accurate expressions of post-fault lines current. Secondly, in order to optimize the parameters of CBs and FCLs, an improved NSGA-II algorithm is proposed in this section.

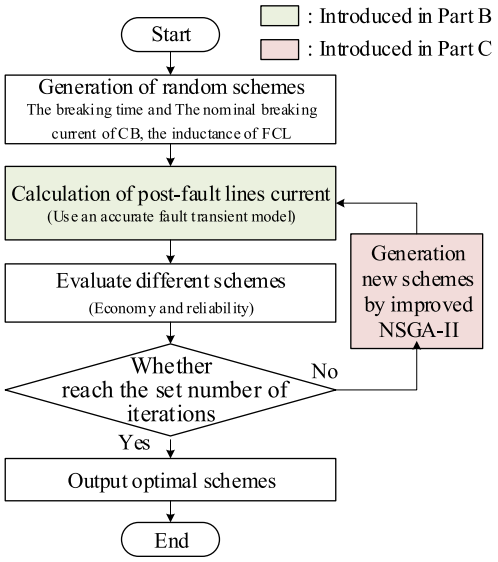

FIGURE 3. Flow chart of parameters selection method of CBs and FCLs.

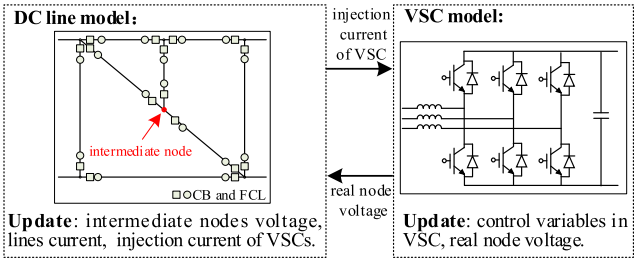

FIGURE 4. Transient model of mesh-type DC microgrid.

A. PROCESS OF PARAMETERS SELECTION METHOD

The flow chart of parameters selection method of CBs and FCLs is shown as Fig. 3. Firstly, the parameter schemes (including the breaking time of CB, the nominal breaking current of CB, the inductance of FCL) are generated randomly. Secondly, the line current under different parameter schemes are obtained based on an accurate post-fault transient model. Furthermore, the economy and reliability of different schemes are evaluated. The economy is the cost of CBs and FCLs in schemes. The reliability is the judgement of whether the current of lines exceeds the nominal breaking current of CBs. Finally, if the set number of iterations is reached, the final schemes are output as the optimal schemes. Otherwise, new parameters schemes are generated by an improved NSGA-II. The innovative work of the post-fault transient model will be introduced in Part B. While, the improvement of NSGA-II will be introduced in Part C.

B. TRANSIENT MODEL OF MESH-TYPE DC MICROGRID

The transient model of mesh-type DC microgrid is shown as Fig. 4, and the model can be divided into DC line model and VSC model. The state variables in mesh-type DC microgrid include lines current, injection current of VSCs, real nodes voltage and intermediate nodes voltage. The lines current, injection current of VSCs, and intermediate nodes voltage are updated in the DC line model. While the real nodes voltage is updated in the VSC model.

The detailed modeling of VSC has been completed in [29], [30]. Since the VSC control system is considered in the modeling, the VSC model becomes a nonlinear system and must be solved in difference equation form instead of differential form. Therefore, in order to obtain the transient model of the entire mesh-type DC microgrid, it is necessary to derive the DC line model in difference equation form.

The DC line model in difference equation form has already been deduced in [29], [30]. However, the DC line model in [29], [30] lacks the consideration of intermediate nodes. Thus, the DC line model considering the intermediate nodes is derived in this part.

1) VARIABLES DEFINITIONS

Assuming that there are n nodes (including N real nodes and M intermediate nodes) and b lines in a mesh-type DC microgrid. Then lines current matrix $\mathbf{i_0}$, VSCs injection current $\mathbf{i_{c0}}$, real nodes voltage matrix $\mathbf{u_{N0}}$, intermediate nodes voltage matrix $\mathbf{u_{M0}}$ and all nodes voltage matrix $\mathbf{u_0}$ in an arbitrary mesh-type DC microgrid can be defined as:

$$\mathbf{i_0}(k) = \left[i_{12}(k) \ \cdots \ i_{ij}(k) \ \cdots\right]_b^T \tag{11}$$

$$\mathbf{i_{c0}}(k) = \left[i_{c1}(k) \ i_{c2}(k) \ \cdots \ i_{cn}(k)\right]_n^T \tag{12}$$

$$\mathbf{u_{N0}}(k) = \left[u_1(k) \ u_2(k) \ \cdots \ u_N(k)\right]_N^T \tag{13}$$

$$\mathbf{u_{M0}}(k) = \left[u_{N+1}(k) \ u_{N+2}(k) \ \cdots \ u_{N+M}(k)\right]_M^T \tag{14}$$

$$\mathbf{u_0}(k) = \left[u_1(k) \ \cdots \ u_N(k) \ u_{N+1}(k) \ \cdots \times \ u_{N+M}(k)\right]_n^T \tag{15}$$

2) DIFFERENCE EQUATIONS OF INTERMEDIATE NODES VOLTAGE

As shown in Fig. 1, intermediate nodes exist only in radial-type topology. Thus, the three-terminal radial-type DC microgrid shown in Fig. 5 is used as an example to analyze the relationship between intermediate nodes voltage and other variables.

The relationship between lines current and nodes voltage in three terminal radial-type DC microgrid can be expressed as:

$$\begin{cases} u_4 = u_1 - L_{14}i'_{14} - R_{14}i_{14} \\ u_4 = u_2 - L_{24}i'_{24} - R_{24}i_{24} \\ u_4 = u_3 - L_{34}i'_{34} - R_{34}i_{34} \\ i_{14} + i_{24} + i_{34} = 0 \end{cases} \tag{16}$$

where u_m is voltage of node m, i_{pq} is current in line p-q and flowing from node p to node q. R_{pq} and L_{pq} are the resistance and inductance of line p-q respectively. Note that R_{qp} and L_{qp} equal to R_{pq} and L_{pq} in this paper.

Eliminating the change rate of current i'_{14}, i'_{24}, i'_{34} in (16), the difference equation of intermediate node voltage u_4 can

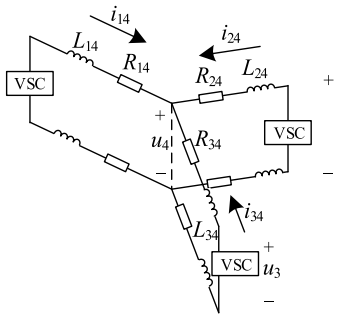

FIGURE 5. Three terminal radial-type DC microgrid model.

be expressed as:

$$u_4(k) = [u_1(k-1)/L_{14} + u_2(k-1)/L_{24} + u_3(k-1)/L_{34} - R_{14} \cdot i_{14}(k-1)/L_{14} - R_{24} \cdot i_{24}(k-1)/L_{24} - R_{34} \cdot i_{34}(k-1)/L_{34}]/(1/L_{14} + 1/L_{24} + 1/L_{34}) \quad (17)$$

where k is iteration step time.

Referring to the derivation of three terminal structure, the difference equations of intermediate nodes voltage in an arbitrary mesh-type DC microgrid in matrix form can be expressed as:

$$\mathbf{A_0} \cdot \mathbf{u_{M0}}(k) = \mathbf{B_0} \cdot \mathbf{u_0}(k-1) - \mathbf{C_0} \cdot \mathbf{i}_0(k-1) \quad (18)$$

where the dimension of $\mathbf{A_0}$ is $M \times M$. The dimension of $\mathbf{B_0}$ is $M \times n$. The dimension of $\mathbf{C_0}$ is $M \times b$.

Since $\mathbf{A_0}$ is a diagonal matrix, the diagonal element A_{ii} can be expressed as:

$$A_{ii} = \sum_{j=1}^{K} (-1)^g / L_{ij} \quad (19)$$

where K is the number of lines connecting to the node. If $j > i$, $g = 2$. Else if $j < i$, $g = 1$.

Each element in $\mathbf{B_0}$ can be expressed as:

$$B_{ij} = \begin{cases} 1/L_{j(i+N)} & \text{exist branch } j-(i+N), j < i+N \\ 0 & \text{none branch } j-(i+N) \end{cases} \quad (20)$$

Each element in $\mathbf{C_0}$ can be expressed as:

$$C_{ij} = \begin{cases} R_b/L_b & \text{exist branch } j-(i+N), j < i+N \\ -R_b/L_b & \text{exist branch } j-(i+N), j > i+N \\ 0 & \text{none branch } j-(i+N) \end{cases} \quad (21)$$

where R_b and L_b are the resistance and inductance of the j th line in $\mathbf{i_0}$ respectively.

3) DIFFERENCE EQUATIONS OF LINES CURRENT AND VSCs INJECTION CURRENT

Since the intermediate nodes voltage can be calculated by (18), the voltage at each node on both sides of a line can be calculated correspondingly. Therefore, the difference equations of each line current can be related to the nodes voltage at both ends of the line. And the difference equations of lines current can be expressed in matrix form as:

$$\mathbf{L_0} \cdot \mathbf{i_0}(k) = \mathbf{L_0} \cdot \mathbf{i_0}(k-1) + \Delta T \cdot [\mathbf{D_0} \cdot \mathbf{u_0}(k-1) - \mathbf{R_0} \cdot \mathbf{i_0}(k-1)] \quad (22)$$

where ΔT is iteration step time. $\mathbf{L_0}$ is an inductor matrix. The dimension of $\mathbf{L_0}$ is $b \times b$. $\mathbf{R_0}$ is a resistor matrix. The dimension of $\mathbf{R_0}$ is $b \times b$. The dimension of $\mathbf{D_0}$ is $b \times n$.

Both the matrix $\mathbf{L_0}$ and $\mathbf{R_0}$ are diagonal matrix. And the value of L_{ii} (R_{ii}) is equal to the inductance (resistance) of the i th line in $\mathbf{i_0}$.

Each element in $\mathbf{D_0}$ can be expressed as:

$$D_{ki} = \begin{cases} 1 & \text{node } i \text{ is the starting point of branch } k \\ -1 & \text{node } i \text{ is the endding point of branch } k \\ 0 & \text{node } i \text{ is not a point of branch } k \end{cases} \quad (23)$$

According to KCL, the relationship between $\mathbf{i_{c0}}$ and $\mathbf{i_0}$ can be expressed as:

$$\mathbf{i_{c0}}(k) = \mathbf{D_0^T} \cdot \mathbf{i_0}(k) \quad (24)$$

4) MODEL MODIFICATION UNDER SHORT CIRCUIT FAULT

Assuming that a short circuit fault occurs in line p-q as shown in Fig. 6, the line p-q is divided into two new lines. The resistance R_{pq} and inductance L_{pq} are replaced by R_{pf}, R_{qf} and L_{pf}, L_{qf} respectively. The faulty position is considered as a new node. And the faulty resistance is R_f. Under this situation, lines current matrix $\mathbf{i_0}$, VSCs injection current $\mathbf{i_{c0}}$ and all nodes voltage matrix $\mathbf{u_0}$ need to be modified as:

$$\mathbf{i}(k) = [i_{12}(k) \cdots i_{pf}(k) \;\; i_{qf}(k) \cdots]^T_{b+1} \quad (25)$$

$$\mathbf{i_c}(k) = [i_{c1}(k) \cdots i_{cn}(k) \;\; i_{cf}(k)]^T_{n+1} \quad (26)$$

$$\mathbf{u_0}(k) = [u_1(k) \cdots u_N(k) \cdots u_n(k) \;\; u_f(k) \;\;]^T_{n+1} \quad (27)$$

The difference equations $\mathbf{u_M}$, $\mathbf{i_0}$, $\mathbf{i_{c0}}$ need to be modified as:

$$\begin{cases} \mathbf{A} \cdot \mathbf{u_M}(k) = \mathbf{B} \cdot \mathbf{u}(k-1) - \mathbf{C} \cdot \mathbf{i}(k-1) \\ u_f(k) = R_f \cdot \mathbf{F} \cdot \mathbf{i}(k-1) \\ \mathbf{L} \cdot \mathbf{i}(k) = \mathbf{L} \cdot \mathbf{i}(k-1) + \Delta T \cdot [\mathbf{D} \cdot \mathbf{u}(k-1) - \mathbf{R} \cdot \mathbf{i}(k-1)] \\ \mathbf{i_c}(k) = D^T \cdot \mathbf{i}(k) \end{cases} \quad (28)$$

where the dimension of $\mathbf{A}$ is $M \times M$. The dimension of $\mathbf{B}$ is $M \times (n+1)$. The dimension of $\mathbf{C}$ is $M \times (b+1)$. i_{pf} and i_{qf} are the current of line p-f and line q-f. $\mathbf{F}$ is a row vector, the dimension of $\mathbf{F}$ is $1 \times (b+1)$, the value of the element corresponding to i_{pf} and i_{qf} is 1, and the value of the remaining elements is

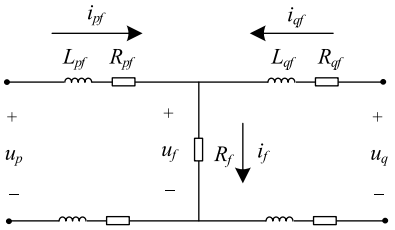

FIGURE 6. An arbitrary fault occurs in line *p-q*.

zero. The dimension of **L** is $(b+1)\times(b+1)$. The dimension of **R** is $(b+1)\times(b+1)$. The dimension of **D** is $(b+1)\times(n+1)$.

Though the dimensions of **A**, **B**, **C**, **L**, **R**, **D** are changed, the selection principles of elements in **A**, **B**, **C**, **L**, **R**, **D** are similar to $\mathbf{A_0}$, $\mathbf{B_0}$, $\mathbf{C_0}$, $\mathbf{L_0}$, $\mathbf{R_0}$, $\mathbf{D_0}$ respectively.

Through the iteration calculation of DC line model and VSC model, the lines current in short circuit fault can be accurately calculated, which provides a basis for optimizing the parameters of CBs and FCLs.

C. IMPROVEMENT OF NSGA-II ALGORITHM

Since there are four optimization objectives of evaluation model, NSGA-II algorithm, which is a multi-objective algorithm, is selected as the optimization algorithm to solve this multi-objective optimization problem. Compared with single-objective algorithm, those four objective functions are independent of each other when solving the multi-objective function, and there is no need to consider the ''weight'' of each optimization objective. Moreover, the NSGA-II algorithm has fast non-dominated sorting, individual crowding distance, elite strategy, etc., which can be referred in [13].

In this paper, three parameters of CBs and FCLs need to be optimized. To avoid the dimensionality disaster caused by too many parameter combinations, the improved NSGA-II algorithm is proposed to accelerate iterative convergence.

1) IMPROVEMENT OF NON-DOMINATED SORTING

The configuration schemes corresponding to individuals, whose E_i in (4) greater than 0, cannot remove all faulty lines reliably. And those schemes will not be adopted as the final configuration schemes. In order to accelerate the convergence, the priority of unsatisfied individuals needs to be lowered. Thus, the non-dominated numbers of those unsatisfied individuals are increased by 1 in this paper.

2) IMPROVEMENT OF CROWDING DISTANCE CALCULATION

The crowding distance of each individual can be expressed as the sum of the crowding distance under each objective function:

$$d_i = \sum_m \frac{f_m(i+1) - f_m(i-1)}{f_m\max - f_m\min}, \quad i \in \{2, 3, \ldots, n-1\} \tag{29}$$

where n is the number of individuals in the set. $f_m(i+1)$ is the objective function m of the $(i+1)$ th individual. $f_m\max$ and $f_m\min$ are maximum number and minimum number of objective function m.

It should be noted that the value of reliability objective function is equal to 0 when the individual meets the requirement for removing the fault reliably, and the crowding distance of this individual is infinity in this condition. With the improvement of non-dominated sorting, the value of reliability objective function of all individuals is 0 in the set with a non-dominated sorting of 1. It means that the crowding distance is useless and cannot inherit individuals with lower density to the next generation. Therefore, the calculation of crowding distance should be improved, and only the crowding distances of the economy objective functions are calculated in this paper.

V. CASE STUDY

In order to validate the accuracy of transient calculation model and the feasibility of parameter selection method, the midpoint of b_{24} (fault condition 1 in Fig. 1) and the terminals of DC lines (fault condition 2 in Fig. 1) are used as analyzed fault position respectively. Moreover, the fault resistance of both fault conditions is zero. The parameters of the mesh-type DC microgrid are given in Section II.A.

A. VALIDATION OF DC MICROGRID TRANSIENT CALCULATION MODEL

The post-fault lines current obtained by the transient calculation model are compared with those obtained by Simulink. And the current of each line obtained by numerical calculation and simulation is shown as Fig. 7.

According to Fig. 7, the closer the line to the faulty position, the larger current change occurs in the line. Since b_{27} and b_{47} connect to faulty position directly, i_{27} and i_{47} are larger than other lines current. The changes of i_{27} and i_{47} are higher than 2000A within 10ms. Since b_{56} stays away from faulty position, i_{56} has the smallest change in all lines current. The change of i_{56} stays in 100A within 10ms. Although the changes of current variations are different, the changes of current errors variations obtained by numerical calculation and EMT simulation are almost consistent. The errors of all lines current keep within 50A within 10ms.

B. VALIDATION OF PARAMETERS SELECTION METHOD

1) BASIC PARAMETERS OF SELECTION METHOD

The basic parameters of selection method include the limit of inequality constraints (shown in Table 5) and the parameters of NSGA-II algorithm (shown in Table 6). Note that calculation with larger value ranges has been done in advance to estimate the value ranges of parameters.

2) COMPARISON OF NSGA-II AND IMPROVED NSGA-II

In order to ensure the persuasiveness of the comparison, except for the two improvements in Section IV.C, the NSGA-II and the improved NSGA-II are the same. The number of optimal schemes which can cut off the faulty line

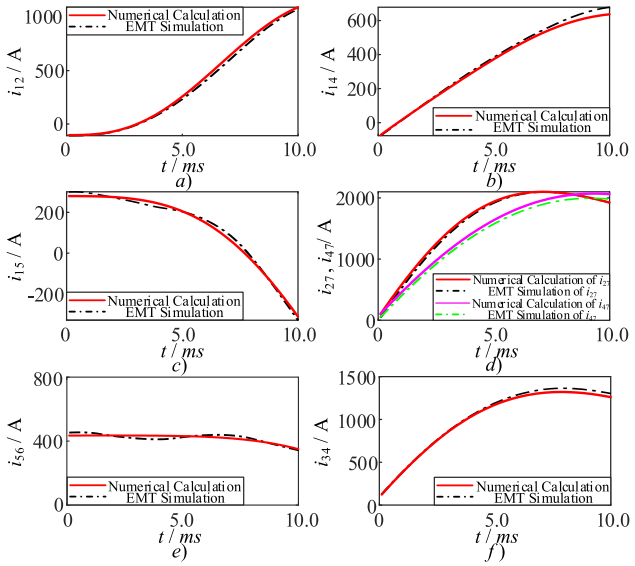

FIGURE 7. Lines current obtain by numerical calculation and EMT simulation. *a*) current of i_{12}, *b*) current of i_{14}, *c*) current of i_{15}, *d*) current of i_{27} and i_{47}, *e*) current of i_{56}, *f*) current of i_{34}.

TABLE 5. The limit of inequality constraints.

Parameter	Lower limit	Upper limit
Breaking time	2ms	12ms
Nominal breaking current	0kA	5kA
Inductance	0mH	5mH
Voltage drop during normal operation		5%
Residual voltage after short circuit	65%	

TABLE 6. The parameters of NSGA-II algorithm.

Parameter	Value	Parameter	Value
Population size	1000	Iterative times	300
Cross rate	0.9	Variation rate	0.1
Accuracy of CBs' breaking time	0.2ms	Accuracy of CBs' nominal breaking current	0.1kA
Accuracy of FCLs' inductance	0.1mH		

reliably is shown in Fig. 8. When NSGA-II is used for solving the problem, the number of optimal schemes keeps changing. The maximum number of optimal schemes is 18 when iterating to 293 times. And the minimum number of optimal schemes is only 4 when iterating to 131 times. The change of the number of optimal schemes means that the optimal schemes may lose in iteration.

After the NSGA-II algorithm is improved, the number of optimal schemes increases as iteration. And 633 optimal schemes are obtained when iterating to 300 times. The increase in the number of optimal schemes effectively avoids the dimensionality disaster and prevents the algorithm from falling into the local optimal schemes.

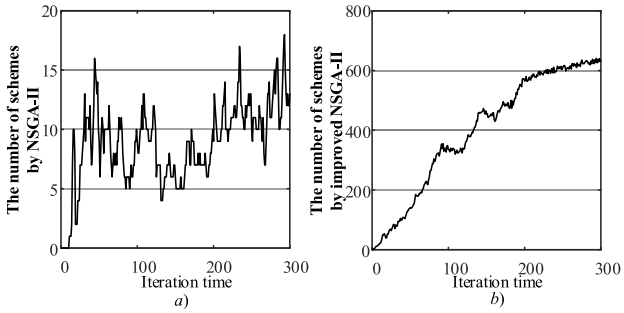

FIGURE 8. The number of schemes which can cut off the line reliably. *a*) obtained by NSGA-II, *b*) obtained by improved NSGA-II.

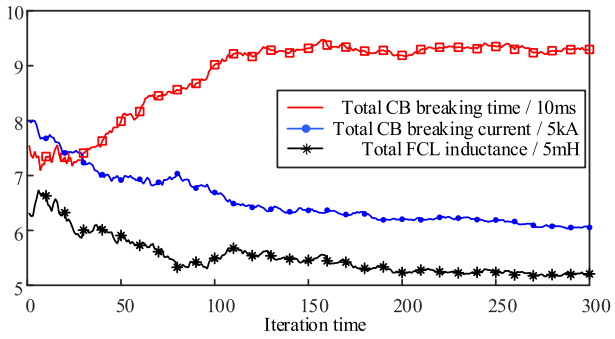

FIGURE 9. The changes of objective functions with iteration.

3) CONVERGENCE OF CBs AND FCLs PARAMETERS

In the process of using NSGA-II to approach optimal scheme set, the total breaking time of CBs gradually increases, the total nominal breaking current of CBs decreases, and the total inductance of FCLs decreases. Thus, the convergence of CBs and FCLs can be obtained by observing the changes of those three objective functions. The changes of objective functions with iteration are shown as Fig. 9. According to Fig. 9, before 150 iterations, the total breaking time of CB raises, while the total nominal breaking current of CB and total inductance of FCL drop. After 150 iterations, those three objective functions remain almost constant and fluctuate over a small range. According to the changes of those three objective functions, the parameters of CBs and FCLs rapidly approximate to the optimal scheme set before 150 iterations and fluctuate around the optimal scheme set after 150 iterations.

4) OPTIMAL SCHEME SET OF CBs AND FCLs PARAMETERS

Through the iterative of NSGA-II, the optimal scheme set can be obtained. And with the help of the optimal scheme set, the Pareto front graph can be fitted out and shown as Fig. 10. It should be noted that through the improvement of NSGA-II in Section IV.C.1), the reliability objective indexes of all the schemes in the optimal scheme set are zero ($f_4 = 0$). So only three economic indexes need to be analyzed.

By observing Fig. 10, it can be found that the Pareto front graph obtained by those three objective functions is a

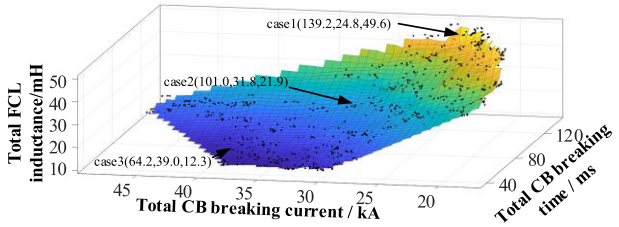

FIGURE 10. The optimal scheme set and the pareto front graph.

TABLE 7. Values of the objective functions for the test system.

	Total CB breaking time / ms	Total CB breaking current / kA	Total FCL inductance / mH
Case 1	139.2	24.8	49.6
Case 2	101.0	31.8	21.9
Case 3	64.2	39.0	12.3

TABLE 8. Values of CBs and FCLs parameters for the test system.

	Line		1-2	1-4	1-5	2-4	3-4	5-6
Case 1	Breaking time of CB/ ms	left	12.0	12.0	12.0	12.0	11.4	11.6
		right	11.6	11.8	8.8	12.0	12.0	12.0
	CB breaking current / kA	left	1.7	3.0	2.1	2.2	2.8	2.1
		right	2.0	2.6	1.6	1.6	1.3	1.8
	Inductance of FCL / mH	left	5.0	4.8	5.0	4.9	5.0	4.7
		right	5.0	0.9	3.7	3.4	2.9	4.3
Case 2	Breaking time of CB/ ms	left	3.6	7.4	5	6.2	8.2	6
		right	7.4	11.8	10	11.4	12	12
	CB breaking current / kA	left	2.1	3.4	3.2	3.3	2.4	2.7
		right	3.4	2.5	1.5	2.7	2.3	2.3
	Inductance of FCL / mH	left	1.6	1.8	1.5	1.9	2.6	2
		right	2.5	0.9	3.5	0.7	0.8	2.1
Case 3	Breaking time of CB/ ms	left	2	2.4	5.8	2.4	3.6	5.4
		right	2	11.6	3.6	10.2	8	7.2
	CB breaking current / kA	left	2.7	3.4	3.8	3.8	2.8	2.4
		right	3.5	2.6	3.4	4	2.5	4.1
	Inductance of FCL / mH	left	0.8	0.7	1.1	0.6	1.7	2.3
		right	0.6	1.2	1	0.3	0.9	1.1

three-dimensional surface, and the non-dominated optimal schemes are distributed on the surface. In the following, three of the obtained results are investigated, denoted as Case 1, Case2 and Case 3. The results of these cases are given in Table 7 and Table 8. And the comparisons of nominal breaking current of CBs and maximum fault current of lines are shown in Fig. 11. Note that the side with a smaller node number is assumed as the left side of a line. The other side is the right side of the line.

According to Table 7, these cases show the optimal choices with different preferences for objective functions. The total breaking time and total nominal breaking current of CB are increased from Case 1 to Case 3, while the inductance of FCL are reduced from Case 1 to Case 3.

As shown in Table 8, the parameters of CBs and FCLs in the three cases are also different. For example, the breaking times of CB on the left side of line 1-2 are 12ms, 3.6ms, 2.0ms respectively. The value in Case 1 is 3.3 times larger than Case 2 and 6 times larger than Case 3.

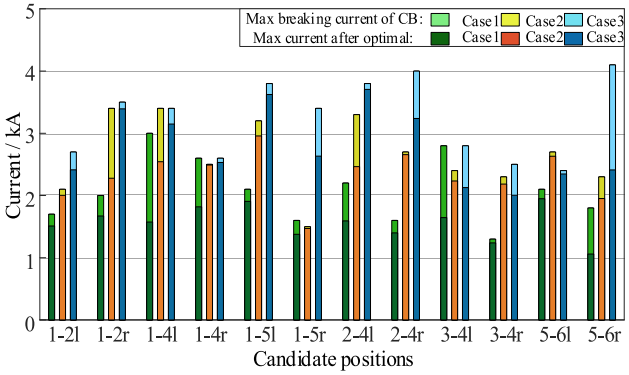

FIGURE 11. Comparison of nominal breaking current of CBs and maximum fault current of lines.

As shown in Fig. 11, although CB and FCL of each candidate position are selected differently by the three cases, all those three cases meet the requirements of cutting off the line reliably.

Moreover, if the cost has a linear relationship with the total nominal breaking current of CB (C_{Total}), the proportional coefficient is 1. If the cost has a linear relationship with the total inductance of FCL (I_{Total}), the proportional coefficient is 1. If the cost is inversely proportional with the total breaking time of CB (T_{Total}), the proportional coefficient is 1000. The relationship between total cost ($Cost_{Total}$) and economic indexes can be expressed as:

$$Cost_{Total} = 1 \times C_{Total} + 1 \times I_{Total} + 1000/T_{Total} \quad (30)$$

With the relationship of (30), the costs of the three cases are: 81.58(Case 1), 63.60(Case 2), 66.88(Case 3). And the optimal scheme is Case 2.

According to the above analysis, it can be known that the optimal scheme set and the Pareto front graph can be obtained by the improved NSGA-II. Besides, in actual application, the optimal scheme can be selected flexibly after getting the relationship between total cost and economic indexes.

VI. CONCLUSION

This paper proposes a parameters selection method of CBs and FCLs in mesh-type DC microgrids. Firstly, all parameters of CBs and FCLs are analyzed and five parameters related to short circuit fault are selected in the evaluation method. Moreover, the post-fault transient model of mesh-type DC microgrid is established to calculate the post-fault current of all lines accurately, in which the intermediate nodes in mesh-type DC microgrids are considered in the proposed method. And then, an improved NSGA-II algorithm, which is improved with the calculation of non-dominated sorting and crowding distance, is provided to optimize the parameters of CBs and FCLs. Besides, the parameters selection method is verified under a modified six-terminal DC microgrid test system. The result shows that the method proposed in this paper can be applied to various faulty DC microgrid analysis, since the method has consideration on both reliability and economy.

REFERENCES

[1] N. Bayati, A. Hajizadeh, and M. Soltani, "Protection in DC microgrids: A comparative review," *IET Smart Grid*, vol. 1, no. 3, pp. 66–75, Oct. 2018.

[2] A. A. A. Radwan and Y. A.-R.-I. Mohamed, "Assessment and mitigation of interaction dynamics in hybrid AC/DC distribution generation systems," *IEEE Trans. Smart Grid*, vol. 3, no. 3, pp. 1382–1393, Sep. 2012.

[3] D. Salomonsson, L. Soder, and A. Sannino, "Protection of low-voltage DC microgrids," *IEEE Trans. Power Del.*, vol. 24, no. 3, pp. 1045–1053, Jul. 2009.

[4] J.-D. Park, J. Candelaria, L. Ma, and K. Dunn, "DC ring-bus microgrid fault protection and identification of fault location," *IEEE Trans. Power Del.*, vol. 28, no. 4, pp. 2574–2584, Oct. 2013.

[5] S. Bifaretti, P. Zanchetta, A. Watson, L. Tarisciotti, and J. C. Clare, "Advanced power electronic conversion and control system for universal and flexible power management," *IEEE Trans. Smart Grid*, vol. 2, no. 2, pp. 231–243, Jun. 2011.

[6] T. Dragicevic, J. C. Vasquez, J. M. Guerrero, and D. Skrlec, "Advanced LVDC electrical power architectures and microgrids: A step toward a new generation of power distribution networks," *IEEE Electrific. Mag.*, vol. 2, no. 1, pp. 54–65, Mar. 2014.

[7] C. Li, C. Zhao, J. Xu, Y. Ji, F. Zhang, and T. An, "A pole-to-pole short-circuit fault current calculation method for DC grids," *IEEE Trans. Power Syst.*, vol. 32, no. 6, pp. 4943–4953, Nov. 2017.

[8] G. Liu, F. Xu, Z. Xu, Z. Zhang, and G. Tang, "Assembly HVDC breaker for HVDC grids with modular multilevel converters," *IEEE Trans. Power Electron.*, vol. 32, no. 2, pp. 931–941, Feb. 2017.

[9] M. Monadi, C. Gavriluta, A. Luna, J. I. Candela, and P. Rodriguez, "Centralized protection strategy for medium voltage DC microgrids," *IEEE Trans. Power Del.*, vol. 32, no. 1, pp. 430–440, Feb. 2017.

[10] R. Mohanty and A. K. Pradhan, "DC ring bus microgrid protection using the oscillation frequency and transient power," *IEEE Syst. J.*, vol. 13, no. 1, pp. 875–884, Mar. 2019.

[11] A. Maqsood and K. Corzine, "DC microgrid protection: Using the coupled-inductor solid-state circuit breaker," *IEEE Electrific. Mag.*, vol. 4, no. 2, pp. 58–64, Jun. 2016.

[12] R. Mohanty and A. K. Pradhan, "Protection of smart DC microgrid with ring configuration using parameter estimation approach," *IEEE Trans. Smart Grid*, vol. 9, no. 6, pp. 6328–6337, Nov. 2018.

[13] L. Kong, H. Nian, Q. Huang, Z. Zhang, J. Xu, and K. Dai, "Optimization of current breaker and fault current limiter in DC micro-grid based on faulty transient analysis," in *Proc. 21st Int. Conf. Electr. Mach. Syst.*, Jeju, South Korea, Oct. 2018, pp. 2017–2022.

[14] J. Liu, N. Tai, and C. Fan, "Transient-voltage-based protection scheme for DC line faults in the multiterminal VSC-HVDC system," *IEEE Trans. Power Del.*, vol. 32, no. 3, pp. 1483–1494, Jun. 2017.

[15] W. Javed, D. Chen, M. Farrag, and Y. Xu, "System configuration, fault detection, location, isolation and restoration: A review on LVDC microgrid protections," *Energies*, vol. 12, no. 6, pp. 1001–1030, 2019.

[16] S. Liu, Z. Liu, J. de Jesus Chavez, and M. Popov, "Mechanical DC circuit breaker model for real time simulations," *Int. J. Electr. Power Energy Syst.*, vol. 107, pp. 110–119, May 2019.

[17] W. Li, Y. Wang, X. Wu, and X. Zhang, "A novel solid-state circuit breaker for on-board DC microgrid system," *IEEE Trans. Ind. Electron.*, vol. 66, no. 7, pp. 5715–5723, Jul. 2019.

[18] A. Shukla and G. D. Demetriades, "A survey on hybrid circuit-breaker topologies," *IEEE Trans. Power Del.*, vol. 30, no. 2, pp. 627–641, Apr. 2015.

[19] T. Nishihara, T. Hoshino, and M. Tomita, "FCL effect of DC superconducting cables in unsteady state," *IEEE Trans. Appl. Supercond.*, vol. 27, no. 4, pp. 1–4, Jun. 2017.

[20] B. Li, J. He, Y. Li, W. Wen, and B. Li, "A novel current-commutation-based FCL for the flexible DC grid," *IEEE Trans. Power Electron.*, vol. 35, no. 1, pp. 591–606, Jan. 2020.

[21] K. Hongesombut, Y. Mitani, and K. Tsuji, "Optimal location assignment and design of superconducting fault current limiters applied to loop power systems," *IEEE Trans. Appl. Supercond.*, vol. 13, no. 2, pp. 1828–1831, Jun. 2003.

[22] S. A. A. Shahriari, A. Y. Varjani, and M. R. Haghifam, "Cost reduction of distribution network protection in presence of distributed generation using optimized fault current limiter allocation," *Int. J. Electr. Power Energy Syst.*, vol. 43, no. 1, pp. 1453–1459, Dec. 2012.

[23] H.-T. Yang, W.-J. Tang, and P. R. Lubicki, "Placement of fault current limiters in a power system through a two-stage optimization approach," *IEEE Trans. Power Syst.*, vol. 33, no. 1, pp. 131–140, Jan. 2018.

[24] P. Chantachiratham and K. Hongesombut, "PSO based approach for optimum fault current limiter placement in power system," in *Proc. 9th Int. Conf. Electr. Eng./Electron., Comput., Telecommun. Inf. Technol.*, May 2012, pp. 1–4.

[25] S. Zare, R. Khalili, A. Khazali, F. Katebi, and S. M. Hashemi, "Fault current limiter optimal placement by harmony search algorithm," in *Proc. 22nd Int. Conf. Exhib. Electr. Distrib.*, Stockholm, Sweden, 2013, pp. 1–4.

[26] T. An, X. Zhou, C. Han, Y. Wu, Z. He, H. Pang, and G. Tang, "A DC grid benchmark model for studies of interconnection of power systems," *CSEE J. Power Energy Syst.*, vol. 1, no. 4, pp. 101–109, Dec. 2015.

[27] R. Bhargav, B. R. Bhalja, and C. P. Gupta, "Algorithm for fault detection and localisation in a mesh-type bipolar DC microgrid network," *IET Gener., Transmiss. Distrib.*, vol. 13, no. 15, pp. 3311–3322, Aug. 2019.

[28] X.-T. Feng, A.-M. Zhang, H. Zhang, J.-J. Huang, and L.-X. Hao, "The integrated control strategy of microgrid based on the voltage source inverter," in *Proc. 33rd Chin. Control Conf.*, Nanjing, China, Jul. 2014, pp. 8222–8227.

[29] H. Nian and L. Kong, "Transient modeling and analysis of VSC based DC microgrid during short circuit fault," *IEEE Access*, vol. 7, pp. 170604–170614, 2019.

[30] L. Kong and H. Nian, "Transient modeling method for faulty DC microgrid considering control effect of DC/AC and DC/DC converters," *IEEE Access*, vol. 8, pp. 150759–150772, 2020.

LIANG KONG received the B.Eng. degree from Zhejiang University, Hangzhou, China, in 2016, where he is currently pursuing the Ph.D. degree in electrical engineering. His research interests include transient analysis and fault protection of dc microgrid.

HENG NIAN (Senior Member, IEEE) received the B.Eng. and M.Eng. degrees in electrical engineering from the Hefei University of Technology, China, and the Ph.D. degree in electrical engineering from Zhejiang University, China, in 1999, 2002, and 2005 respectively.

From 2005 to 2007, he held a postdoctoral position with the College of Electrical Engineering, Zhejiang University, where he was promoted to an Associate Professor, in 2007. From 2013 to 2014, he was a Visiting Scholar with the Department of Electrical, Computer, and System Engineering, Rensselaer Polytechnic Institute, Troy, NY, USA. Since 2016, he has been a Full Professor with the College of Electrical Engineering, Zhejiang University. He has published more than 20 IEEE/IET transaction articles and holds more than 20 issued/pending patents. His current research interests include the optimal design and operation control for wind power generation systems.